Catena 172 (2019) 54–64

Contents lists available at ScienceDirect

Catena

journal homepage: www.elsevier.com/locate/catena

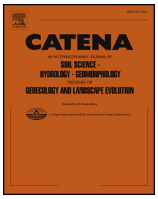

Mineralogy, petrography and geochemistry of an early Eocene weathering profile on basement granodiorite of Qaidam basin, northern Tibet: Tectonic and paleoclimatic implications

Xing Jian[a,*], Wei Zhang[a], Hanghai Liang[a], Ping Guan[b], Ling Fu[c]

[a] State Key Laboratory of Marine Environmental Science, College of Ocean and Earth Sciences, Xiamen University, Xiamen 361102, PR China
[b] MOE Key Laboratory of Orogenic Belts and Crustal Evolution, School of Earth and Space Sciences, Peking University, Beijing 100871, PR China
[c] Research Institute of Petroleum Exploration and Development (RIPED), PetroChina, Beijing 100083, PR China

ARTICLE INFO

Keywords:
Chemical weathering
Climate
Tectonics
Element mobility
Sediment provenance

ABSTRACT

Weathering, as an important process in the earth surface system, can be significantly influenced by tectonics and climates over long time scales. Here, we use mineralogical, petrographic and geochemical data of a paleoweathering profile developed on basement granodioritic rocks of northern Qaidam basin, northern Tibet, to reconstruct early Eocene weathering conditions and to discuss how paleoclimates and tectonics dominated the weathering process. The results indicate that neoformed mineral phases in weathering products are dominated by smectite, and the profile has overwhelmingly low chemical index of alteration values (ca. 51–59) and significantly decreasing micropetrographic index values (from 25.0 to 0.2) from bottom to top. These findings suggest that the basement rocks experienced mild chemical weathering but relatively intensive physical weathering. We favor that non-steady-state weathering, in which mechanical erosion rates compare favorably with rates of chemical weathering, prevailed in northern Tibet during the early Eocene. The weathering conditions were likely an integrated response to active tectonism and dry climates at that time. Furthermore, chemical element mobility evaluation demonstrates that most of large ion lithophile elements and light rare earth elements (LREEs) of granodioritic rocks are quite active during weathering and can be easily leached even under mild chemical weathering conditions. Significant mass loss of Al and LREEs in upper weathered samples probably reflects acidic weathering conditions, which were likely due to extremely high atmospheric CO_2 level during the early Eocene. This study, from the unique perspective of weathering process, suggests that intensive deformation and rapid tectonic erosion occurred in northern Tibet during the early Eocene, as a far-field response to the India-Eurasia collision. It also agrees with warm and relatively dry climates, which were likely attributed to the global greenhouse climates and the Paleogene planetary-wind-dominant climate system in Asia, respectively.

1. Introduction

Chemical weathering is a crucial process to control the evolution of the earth surface system, by shaping landscapes, supplying nutrients and trace elements from lithosphere to biosphere and regulating global chemical cycles. Silicate weathering in particular effects the global carbon cycle and thereby global climate through the consumption of atmospheric CO_2 that is eventually stored as carbonates in the oceans (Berner, 1995; Kump et al., 2000). Therefore, chemical weathering of silicate rocks is generally regarded as an important sink of atmospheric CO_2 over geologic timescales and has attracted considerable attention for decades (e.g. White and Blum, 1995; Gaillardet et al., 1999; West et al., 2005; Misra and Froelich, 2012).

It is well accepted that climatic (e.g. temperature, precipitation and runoff), tectonic (e.g. relief, uplift, exhumation and physical erosion) and internally lithological (e.g. ultramafic, mafic and felsic) factors serve as principal controls on weathering process over different time scales (e.g. Raymo and Ruddiman, 1992; Bluth and Kump, 1994; White and Blum, 1995; Riebe et al., 2001; Jacobson et al., 2003; West et al., 2005; Dixon et al., 2012). In this case, paleoweathering study can offer a unique perspective to evaluate and reconstruct tectonic and climatic conditions during the earth's history.

Several approaches can be applied to investigate paleoweathering and associated controlling factors. While elemental and isotopic

---

* Corresponding author.
E-mail address: xjian@xmu.edu.cn (X. Jian).

https://doi.org/10.1016/j.catena.2018.07.029
Received 8 February 2018; Received in revised form 18 July 2018; Accepted 22 July 2018

geochemistry data of paleo-seawater have been usually used to reconstruct the global chemical weathering rates during the earth's history (Hodell et al., 1991; Lear et al., 2003; Foster and Vance, 2006; Misra and Froelich, 2012), ancient siliciclastic sediments have been often taken as research objects to evaluate paleoweathering intensity of their source regions (e.g. Nesbitt and Young, 1982; McLennan, 1989; Condie, 1993; Nesbitt et al., 1997; Jian et al., 2013b). However, caution should be exercised while using sediment compositional (e.g. mineralogical and geochemical) proxies to track paleoweathering history, since several factors in addition to chemical weathering might influence sediment compositions during the whole source-to-sink process, such as complicated paleodrainage system, contribution of multiple sources, sorting of detrital minerals and diagenetic alteration (Condie et al., 1995; Fedo et al., 1995; Nesbitt et al., 1996; Garzanti et al., 2010; Jian et al., 2013b). Study on a paleoweathering profile could avoid these effects, which is able to provide in-place data for evaluating weathering conditions during the development of the profile. Hence, paleoweathering profiles have been often concerned and investigated to reconstruct tectonic and climatic history during the earth evolution (e.g. Holland and Beukes, 1990; Nedachi et al., 2005; Driese et al., 2011).

The early Eocene, commonly referred to as the Early Eocene Climatic Optimum (Zachos et al., 2001), was a crucial period during the Cenozoic. The earth then was characterized by high atmospheric CO_2 levels (> 1000 ppmv) (Pagani et al., 2005; Lowenstein and Demicco, 2006) and greenhouse climates (Sloan and Rea, 1995; Zachos et al., 2001, 2008). Meanwhile, the Indian and Eurasian plates collided (at ca. 55–50 Ma), which has been regarded as one of the most significant tectonic events on the earth during the Cenozoic. Subsequently intensive deformation, crustal thickening and uplift generated high-relief topography over a region of approximately 3 million km^2, i.e. the Tibetan Plateau (Yin and Harrison, 2000). It is well known that the early Eocene northern Tibet had regionally dry climates and was in active tectonic settings (e.g. Wang et al., 1999; Sun and Wang, 2005; Yin et al., 2008a; Clark et al., 2010; Zhuang et al., 2011; Yuan et al., 2013; Jian et al., 2018). Although previous studies suggest that intensified chemical weathering of continental silicates prevailed and the ocean environment was drastically perturbed during the Paleocene–Eocene thermal maximum (Robert and Kennett, 1994; Zachos et al., 2005), how the climates and tectonics controlled the early Eocene weathering in the northern Tibet remains elusive questions.

In this study, we focus on a well-preserved granodioritic paleoweathering profile underlain by Cenozoic sedimentary rocks of the Qaidam basin, northern Tibet (Fig. 1), and present mineralogical, petrographic and geochemical data and corresponding interpretations. The aims are to: (1) evaluate weathering conditions in northern Tibet during the early Eocene and (2) explain how the tectonics and paleoclimates influenced surface weathering over a geologic timescale.

2. Geological setting

The Cenozoic Qaidam basin is the largest sedimentary basin in the northern Tibetan Plateau and sits 2.7–3 km above sea level. It is currently located in a very active tectonic background and is bounded by three large mountain ranges (i.e. Eastern Kunlun, Qilian and Altun Mountains) which stand up to 5 km above sea level (Fig. 1A–B). The formation of the current basin-range system is a result of on-going convergence between the Indian and Eurasian plates (Yin and Harrison, 2000; Yuan et al., 2013). Although most structures in the north margin of the plateau have been proven to initiate since the middle Miocene, evidence accumulated recently suggests that widespread deformation and rapid exhumation occurred during the early Eocene (Yin et al., 2008a; Clark et al., 2010; Zhuang et al., 2011; Jian et al., 2018) and the northern boundary of the plateau was established once the India-Eurasia collision commenced (e.g. Yuan et al., 2013 and reference therein).

The current Qaidam basin, as a part of the western China, has dry and cold climates due to high elevations, long distances away from oceans and the Asia monsoon system (Molnar et al., 1993; An et al., 2001; Sun and Wang, 2005). Previous pollen, paleobotanical, sedimentological and geochemical evidence demonstrates that the Eocene Qaidam basin had arid to semiarid climates (Wang et al., 1999; Sun and Wang, 2005; Wang et al., 2011; Guo et al., 2017). Evaporite layers (such as halite and gypsum) are widely distributed in the Eocene sedimentary strata of the basin (Wang et al., 2011; Guan and Jian, 2013; Guo et al., 2017). The regionally dry conditions are commonly suggested to be governed by the Paleogene planetary-wind-dominant climate system, which resulted in a zonal arid band extending from East China to Central Asia (Liu and Guo, 1997; Sun and Wang, 2005; Zhang et al., 2007). Besides, given the global greenhouse climate (e.g. Sloan and Rea, 1995; Zachos et al., 2001, 2008) and the paleo-latitude of ca. 30° N based on paleomagnetic measurements (Wu et al., 1997), the Qaidam basin probably had relatively warm climates during the early Eocene.

The Paleogene strata of the Qaidam basin include the following stratigraphic units: 1) Lulehe Formation (E_{1+2}, ~53.5–~46 Ma); 2) Xia Ganchaigou Formation (E_3, ~46–~35.5 Ma, can be divided into lower and upper parts, i.e., E_3^1 and E_3^2); 3) Shang Ganchaigou Formation (N_1, ~35.5–~22 Ma) (e.g. Jian et al., 2013a; Ji et al., 2017). Both outcrop geological mapping and hydrocarbon exploration drilling data indicate that the Paleogene mainly unconformably lies on Jurassic–Cretaceous sedimentary strata or contacts with pre-Cenozoic basement by faults (Guan and Jian, 2013 and reference therein). Although E_{1+2} strata are widely distributed in the basin (e.g. Yin et al., 2008b), the Maxian paleohigh (Fig. 1C), where the pre-Cenozoic crystalline basement is directly underlain by E_3^1 strata (Fig. 1D; Fig. 2), is supposed to be one of the few exposed areas within the basin area during the early Eocene (Guan and Jian, 2013; Jian et al., 2018). Weathered basement crystalline rocks and overlying E_3^1 sedimentary rocks were fortunately and continuously collected along with the drilling of the hydrocarbon exploration Well MB14 in this area (Fig. 1C–D). Hence, rock cores from Well MB14 provide ideal materials for early Eocene weathering profile investigation.

3. Sample collection and analytical methods

The obtained weathering profile is 3.5 m in length and can be macroscopically divided into four layers with different alteration degrees (Fig. 2), including a 0.4 m saprolite layer (Layer 4), fractured and slightly weathered bedrock (1.1 m, Layer 3), slightly weathered to fresh bedrock (1.5 m, Layer 2) and fresh bedrock (0.5 m, Layer 1). Eight samples were collected along the weathering profile (Fig. 2).

The samples were made to thin-sections for petrographic study. Modal analysis of seven selected samples was carried out using point-counting method and ca. 400 points were counted for each sample. Samples for mineralogical and geochemical analysis were first crushed and then powdered to 200 mesh with an agate mortar.

A Rigaku Ultima IV X-ray diffractometer (XRD) at Xiamen University was used for whole-rock mineral and total clay fraction (< 2 μm) composition analysis. The < 2 μm particles were separated following the Stoke's law and were concentrated using a centrifuge. The resulting pastes were then air-dried on glass slides before XRD scanning. Each sample was continuously scanned under 40 kV, 30 mA, wave length of 1.54 and step width of 0.02° conditions. Scanning speeds were 4°/min and 2°/min for whole rock analysis and < 2 μm fraction analysis, respectively. A MDI jade software was employed for data smoothing, peak picking and phase identification.

Major element compositions were determined by an X-ray fluorescence (XRF) spectrometer at the Research Institute of Uranium Geology (Beijing). The sample powders and lithium metaborate flux were mixed in 1:10 and fused at 1050 °C in a Pt—Au crucible. The well-mixed melt was cooled and then a glass disk was made for XRF analysis. The loss on ignition (LOI) values were obtained by measuring the weight loss after heating the sample at 980 °C.

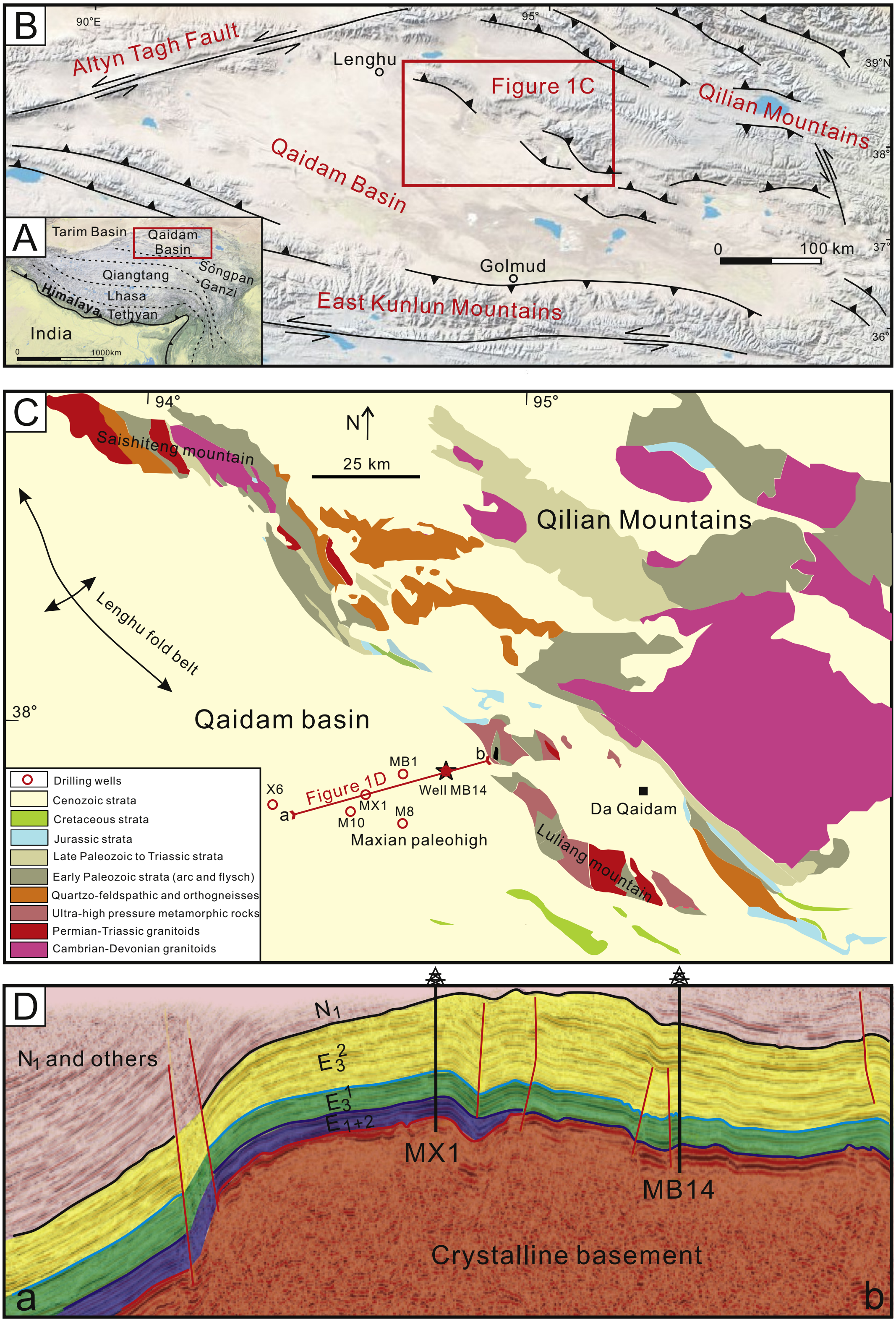

Fig. 1. Maps of the Tibetan Plateau (A) and northern Tibet (B) showing locations of the Qaidam basin and surrounding tectonic elements. (C) Location and geological settings of the paleoweathering profile (drilling well MB14). (D) A representative seismic profile showing spatial distribution of the Paleogene sedimentary strata in the Maxian paleohigh area. E_{1+2}: Lulehe Formation, E_3^1: lower Xia Ganchaigou Formation, E_3^2: upper Xia Ganchaigou Formation, N_1: Shang Ganchaigou Formation.

Trace and rare earth element compositions were analyzed using an ELEMENT ICP-MS at the Research Institute of Uranium Geology (Beijing). Prior to the mass spectrum analysis, the sample powders were accurately weighed (25 mg) and completely dissolved by HF-HNO$_3$-HClO$_4$ mixture acid solutions in high-pressure-resistant Teflon beakers. The detailed analytical procedures were given in Jian et al. (2013b). For the major, trace and rare earth element geochemical analysis, international standards of GSR-4 and GSR-5 were used to monitor

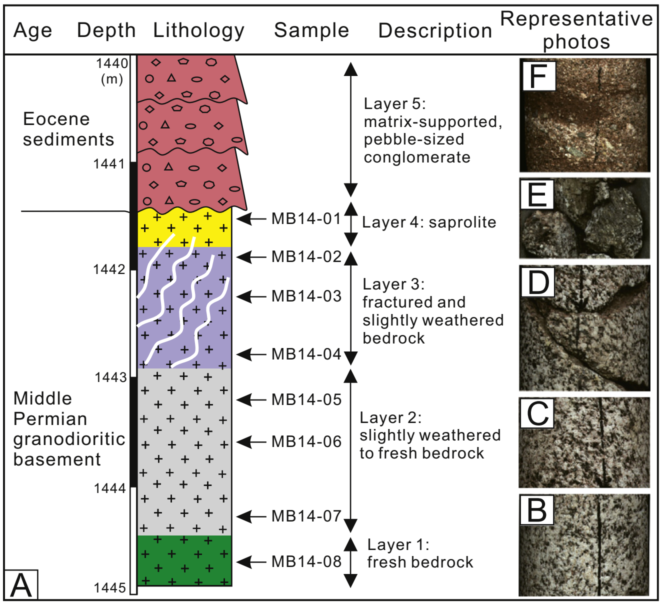

Fig. 2. (A) Lithological descriptions of the paleoweathering profile and sample locations. (B), (C), (D), (E) and (F) representative photographs of the fresh bedrock (1444.8 m), slightly weathered to fresh bedrock (1443.2 m), fractured and slightly weathered bedrock (1442.3 m), saprolite (1441.5 m) and overlying conglomerate (1441.1 m). The granodioritic rocks are supposed to be formed under a subduction-related arc background during the Middle Permian, with the zircon U—Pb age of 271 ± 2 Ma (Cheng et al., 2017).

analytical quality. The accuracy was estimated to be < 2% for all major element oxides (except MnO (4%)), < 10% for all trace elements except Co (19%) and Be (15%).

4. Results

4.1. Petrography

Petrographic observations indicate that the profile is composed of coarse-grained granodioritic rocks. Fresh samples primarily consist of plagioclase, quartz, biotite and K-feldspar, while accessory minerals include hornblende, sphene, zircon and chlorite. Samples from Layer 2 are characterized by slight plagioclase sericitization (Fig. 3E–F), while samples from Layer 3 are featured by different degrees of plagioclase sericitization and abundant microfractures and voids (Fig. 3B–D). The saprolite sample (i.e. Sample MB14–01) shows strong alterations (Fig. 3A) but the granodioritic texture remains. Point counting-based modal compositions of the analyzed samples are shown in Table 1. The results reveal relatively low abundances of plagioclase and biotite, and high fracture proportions in the upper samples. Sample MB14–02, which is located at the top of Layer 3, has the most abundant (31.6%) microfractures and voids (Table 1, Fig. 3B).

4.2. Mineral compositions based on XRD analysis

The whole-rock XRD analysis results of six selected samples and total clay fraction (i.e. < 2 μm) XRD patterns of three upper samples are shown in Fig. 4. Diffraction patterns of the whole-rock powder samples show consistently strong peaks of quartz and plagioclase in lower samples, and demonstrate decrease of plagioclase abundances in upper weathered samples. Furthermore, the upper samples (in particular Sample MB14–01) have new peaks (d = 9.1 Å; Fig. 4A), which can be identified as barrerite (Fig. A1 in the Supplementary Material). The < 2 μm fractions of the analyzed upper samples are dominated by smectite, with subordinate illite (Fig. 4B).

4.3. Major element compositions

Major element geochemical data are shown in Table A.1 (in the Supplementary Material) and are illustrated with depths in Fig. 5A. The fresh and slightly weathered to fresh bedrocks have high SiO_2

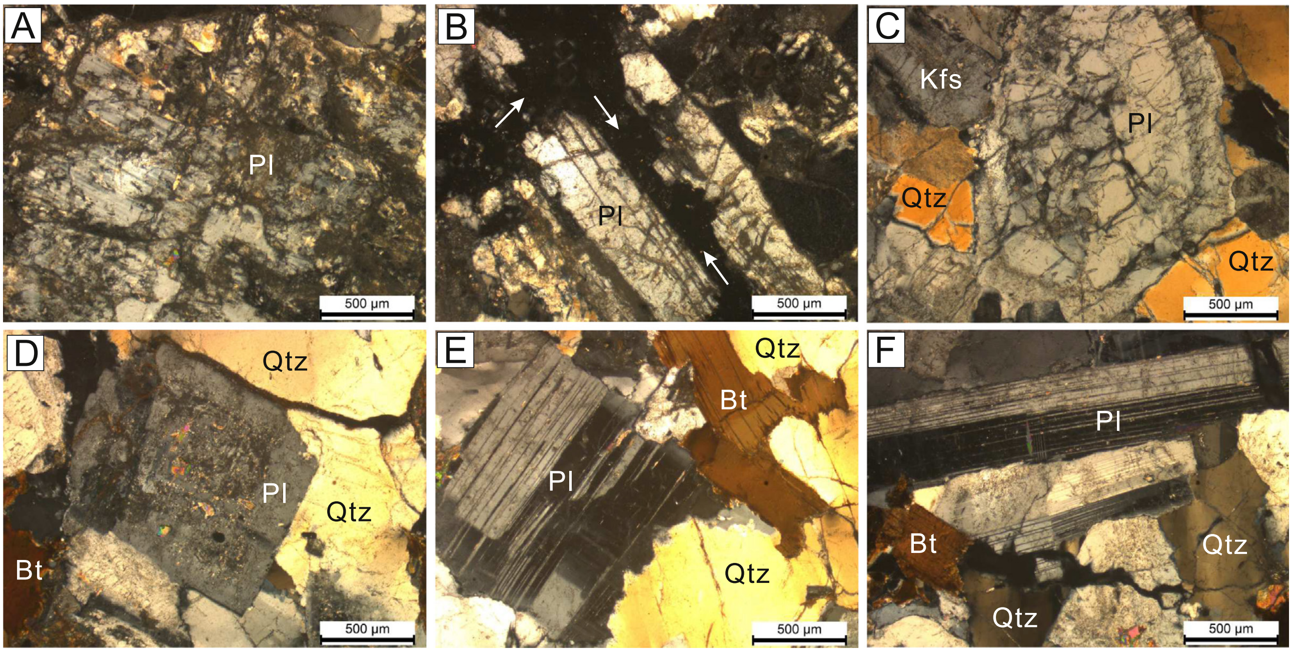

Fig. 3. Representative photomicrographs of the analyzed samples. (A) the plagioclase grain was significantly altered (Sample MB14–01); (B) Sample MB14–02 is characterized by abundant fractures (white arrows); (C) intensive microfractures within plagioclase and quartz grains (Sample MB14–03); (D) slightly weathered plagioclase (Sample MB14–04); (E) and (F) slightly weathered granodioritic bedrocks (Samples MB14–06 and MB14–07, respectively). Qtz: quartz, Pl: plagioclase, Kfs: K-feldspar, Bt: biotite. All the photomicrographs were taken under the cross-polarized light.

Table 1
Petrographic modal compositions and micropetrographic index (Ip).

Sample	Modal compositions based on point-counting data						Micropetrographic index calculation		
	Qtz	Pl	Kfs	Bt	Others	Microfractures and voids	Unweathered	Weathered	Ip
MB14–01	25.3	20.9	2.2	7.7	30.8	13.2	18.7	68.1	0.23
MB14–02	24.1	26.6	2.5	8.7	6.5	31.6	21.5	46.8	0.27
MB14–03	25.0	50.0	4.3	6.5	2.2	12.0	41.3	46.7	0.70
MB14–04	20.0	56.0	3.0	12.0	3.0	6.0	74.0	20.0	2.85
MB14–06	22.0	58.7	1.8	11.0	1.8	4.6	93.6	1.8	14.57
MB14–07	21.1	56.8	3.2	12.6	2.1	4.2	93.7	2.1	14.83
MB14–08	21.2	55.8	3.8	12.5	3.8	2.9	96.2	1.0	25.00

The modal data are in volume percent. The micropetrographic index (Ip) was proposed by Irfan and Dearman (1978). Qtz: quartz, Pl: plagioclase, Kfs: K-feldspar, Bt: biotite, Unweathered: unweathered primary minerals, Weathered: weathered minerals including neoformed phases, Ip = unweathered/(weathered + microfractures and voids). Others mainly include accessory minerals (e.g. hornblende, sphene, zircon and chlorite) and neoformed minerals.

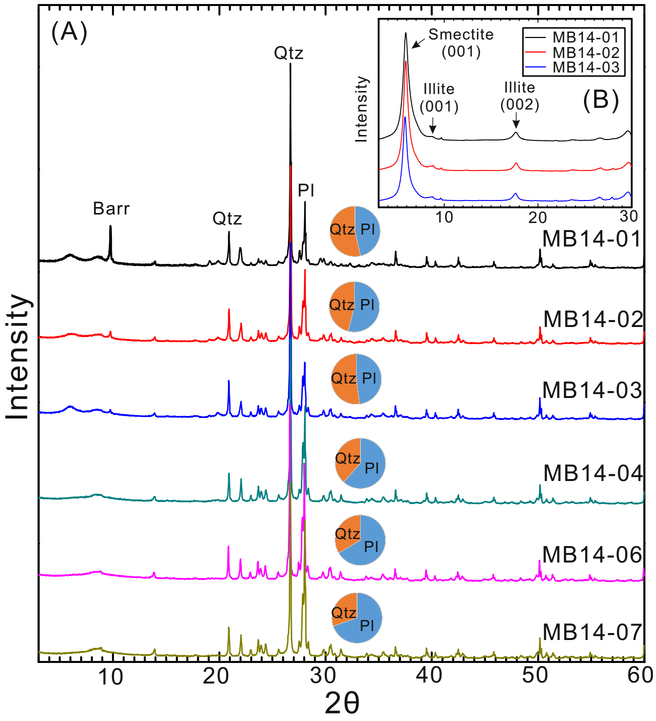

Fig. 4. Whole-rock (A) and clay mineral fraction (B) XRD analysis results of selected samples. Pie charts indicate relative abundances between quartz and plagioclase based on XRD pattern interpretations. Note that the upper weathered samples have relatively low abundances of plagioclase, barrerite is not significantly present in the < 2 μm fractions and neoformed minerals are dominated by smectite. Qtz: quartz, Pl: plagioclase, Barr: barrerite.

(65.11–65.33 wt%), Al_2O_3 (17.04–17.50 wt%), CaO (3.94–4.31 wt%) and Na_2O (3.95–4.11 wt%) contents and low Fe_2O_3(T), K_2O, MgO, MnO, TiO_2 and P_2O_5 contents, as well as relatively low LOI values (1.43–1.71 wt%). All the samples have relatively constant Ti and P contents. The upper samples of the profile have higher LOI values (up to 5.31 wt%) and show significant depletion in Ca and Na, slight depletion in Al, and obvious enrichment of Fe and Mn (Fig. 5A).

4.4. Trace- and rare earth element compositions

Trace- and rare earth elemental data are shown in Table A.1 (in the Supplementary Material). Fig. 5B indicates the variations of representative trace and rare earth element (REE) contents with sampling depths. The results demonstrate that the upper weathered samples display remarkable depletion in Be, Sr and Ba, while the contents of Th, Sc, Cr, Nb, Y and most REEs (except La and Ce) have no obvious correlations with depths (Figs. 5–6). It is worth noting that some trace elements (e.g. Th, Sc, Nb, Eu, Zr and Hf) reveal highly variable abundances in the three slightly weathered to fresh bedrock samples (Table A.1). Although the analyzed samples have fluctuant total contents of REEs (64.8–122.7 ppm), the chondrite-normalized patterns are roughly consistent (except Ce) among the samples of different depths (Fig. 6). Compared with the lower samples, the upper samples show positive Ce anomalies (chondrite-normalized, with the Ce/Ce* ranges from 1.19 to 1.50) and have relatively low La contents and La_N/Yb_N values (Table A.1).

5. Interpretation and discussion

5.1. Alteration and weathering intensity of the early Eocene weathering profile

Petrographic observation results (Figs. 2–3) indicate well-developed macro-cracks and intragranular microfractures in the upper weathered samples of the profile, implying relatively extensive disintegration and thus intensive physical alteration of the basement granodiorite. The decrease of plagioclase in the upper weathered samples and significant peaks of smectite in the < 2 μm fraction XRD patterns (Fig. 4) suggest that conversion of plagioclase to smectite was likely to dominate the chemical weathering process on the profile. It is well known that smectite can be one kind of neoformed weathering products of plagioclase, although other mineral phases, such as kaolinite, gibbsite and several forms of halloysite, can also be involved in (Banfield and Eggleton, 1990; Wilson, 2004), depending on weathering conditions and degrees (e.g. Aoudjit et al., 1995; Nesbitt et al., 1997). Furthermore, barrerite, which is known as a sodium-rich zeolite (the ideal chemistry is $(Na, K, Ca)_2Al_2Si_7O_{18}{\cdot}7H_2O$) of the stilbite group, is present in the upper layers of the profile (Fig. 4A). The barrerite is extremely uncommon in the world and is usually known to form under post-magmatic hydrothermal alteration (e.g. Ghobarkar et al., 1999; Pe-Piper, 2000; Fuentes et al., 2004; Gottardi and Galli, 2012). In addition, it can also be formed by direct crystallization in the presence of Na-rich seawater (e.g. Di Renzo and Gabelica, 1997). In this study, we infer that the barrerite was generated due to possible Na-rich fluids percolating through upper part of the bedrock, since the Cenozoic northern Qaidam basin was in continental environments (Zhuang et al., 2011; Guan and Jian, 2013) and we can't find any evidence to support post-magmatic hydrothermal alteration.

Weathering indices are useful tools in characterizing weathering profiles and quantifying the degree of weathering. Various weathering indices based on petrographic and geochemical data have been proposed by many researchers for over the years (e.g. Irfan and Dearman, 1978; Nesbitt and Young, 1982; Fedo et al., 1995; Price and Velbel, 2003 and references therein). The Micropetrographic Index (Ip), devised by Irfan and Dearman (1978), is defined as a ratio among unweathered primary minerals and weathered minerals (also including

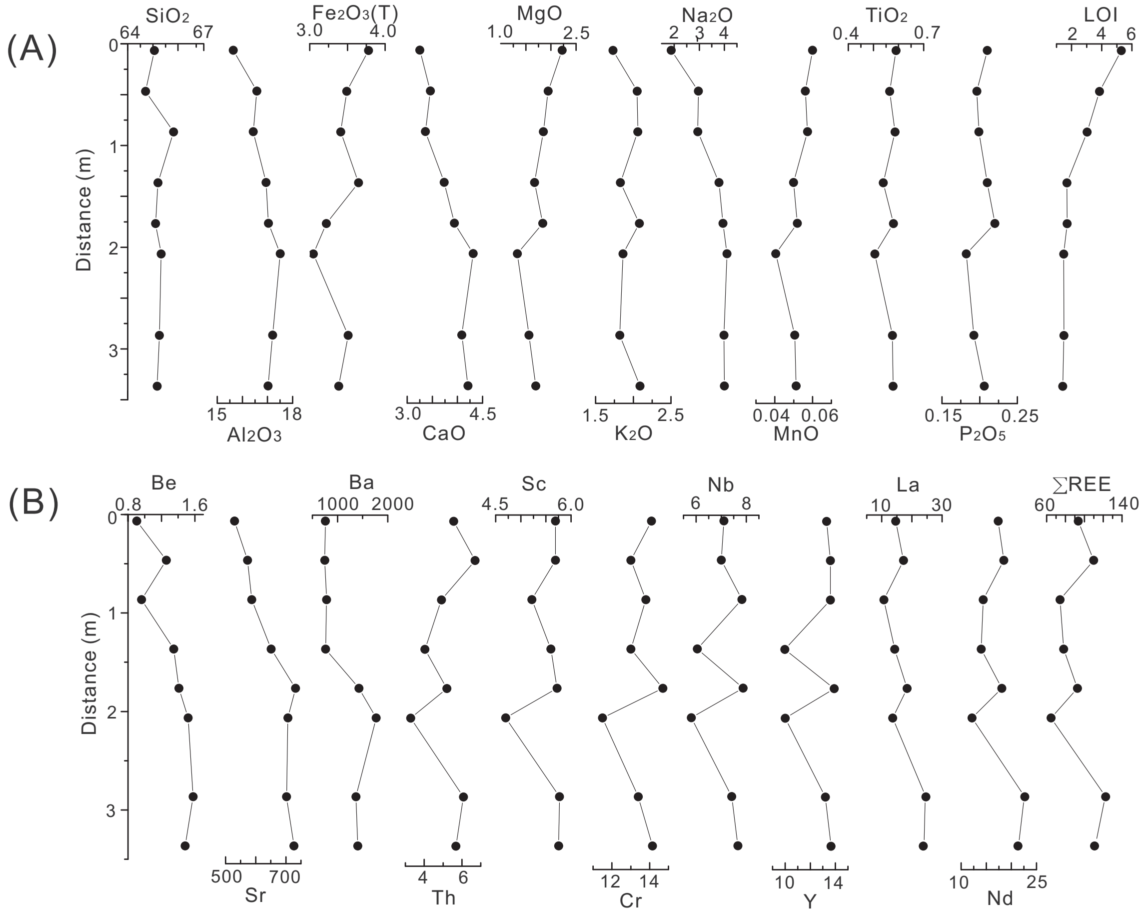

Fig. 5. (A) Vertical variations of the major element compositions (in wt%) along the paleoweathering profile. (B) Vertical variations of representative trace- and rare earth element compositions (in ppm) along the profile. The vertical axis indicates the distance below the surface of the profile.

secondary phases together with microcracks and voids), and thus tends to decrease as far as weathering goes on. The Chemical Index of Alteration (CIA), proposed by Nesbitt and Young (1982), is calculated as the ratio $[Al_2O_3/(Al_2O_3 + CaO + Na_2O + K_2O)*100]$ in molecular proportions, where CaO represents Ca content in silicate minerals only. The CIA has been widely used to quantify degree of chemical weathering for (paleo-) weathering profiles and to reconstruct source region chemical weathering conditions for ancient and modern sediments. The Plagioclase Index of Alteration (PIA), is calculated as the ratio $[(Al_2O_3–K_2O)/(Al_2O_3 + CaO + Na_2O–K_2O)*100]$ in molecular proportions, was proposed by Fedo et al. (1995) to unravel the effects of K-metasomatism in sedimentary rocks and paleosols. Since the fresh bedrock samples have abundant plagioclases (Table 1, Fig. 3), the PIA is favored for chemical weathering evaluation of plagioclase in this study. Both the CIA and PIA values tend to increase along with increasing weathering degrees and these ratio calculations yield values of ca. 50 for fresh rocks and values close to 100 for final products of weathering, i.e. clay minerals such as kaolinite, chlorite and gibbsite. Furthermore, the ratios between plagioclase and quartz contents (Pl/Qtz ratios, based on petrographic data) are also calculated.

The results are shown in Table 1 and Fig. 7. The Pl/Qtz ratios, CIA and PIA values vary from 2.8 to 0.83, from 50.8 to 59.0 and from 50.9 to 60.4, respectively. Note that the CIA and PIA values of the uppermost sample (i.e. MB14–01) might be a little bit underestimated because the presence of barrerite (barrerite has CIA and PIA values of ca. 50) which is possibly due to Na-rich fluid percolation rather than silicate weathering. Although the point-counting-based Pl/Qtz ratios display obvious decrease from bottom to top weathered samples, the petrographic results indicate slightly chemical alterations on the plagioclase (Fig. 3). The upper weathered samples only have slightly higher CIA and PIA values than the fresh bedrock sample, implying that the basement crystalline rocks underwent mild chemical weathering during the early Eocene. The presence of smectite, as the major neoformed mineral in weathering products (Fig. 4B), also reveal immature chemical weathering of plagioclase (Banfield and Eggleton, 1990; Wilson, 2004). However, the Ip values of the samples vary from 14.83 to 0.23, and the upper weathered samples have abundant intragranular microfractures and voids and show much lower Ip values than the fresh bedrock sample (Table 1; Fig. 7). Note that both physical and chemical weathering can result in decrease of the Ip values (Irfan and Dearman, 1978). This means physical weathering (such as mechanical breakdown and disintegration of rocks) contributed most extent of the basement weathering and resulted in much lower Ip values of the upper samples (Fig. 7). Collectively, we conclude that the basement granodioritic rocks experienced mild chemical weathering but relatively intensive physical weathering during the early Eocene.

5.2. *Evaluation of chemical element mobility*

We assume no chemical loss or gain for fresh bedrock. Elements such as Zr and Ti are usually regarded to be chemically immobile during bedrock weathering (Nesbitt, 1979; Braun et al., 1993). Tau (τ_i) values, which represent the fractional mass gain ($\tau > 0$) or loss ($\tau < 0$) relative to unweathered bedrock material, are commonly used to quantify the changes in elemental concentrations that occur with weathering (e.g. Dixon et al., 2012; Berger et al., 2014). τ_i values can be calculated as:

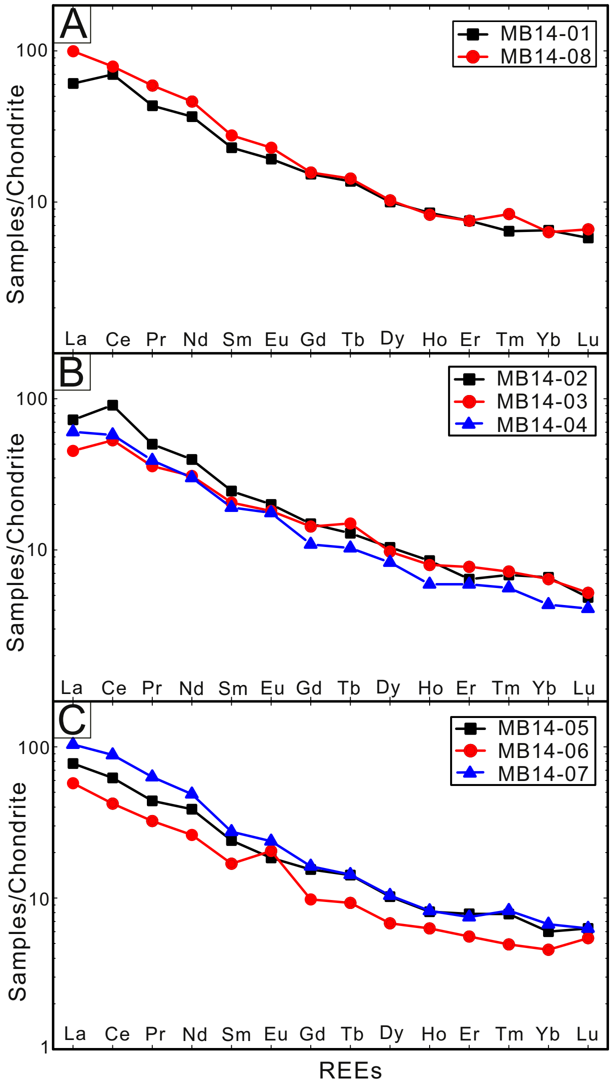

Fig. 6. Chondrite-normalized REE patterns of the analyzed samples. Note that Sample MB14–06 shows positive Eu anomaly and the upper weathered samples have obviously positive Ce anomalies. Compositions of the CI carbonaceous chondrite (McDonough and Sun, 1995) are employed for the normalization.

$$\tau_i = \left(\frac{i_{sample} \times Ti_{bedrock}}{i_{bedrock} \times Ti_{sample}} - 1\right) \qquad (1)$$

where Ti is selected to represent an immobile element, i_{sample} and i_{bedrock} are concentrations of element i in the weathered samples and unweathered bedrock samples, respectively, and Ti_{sample} and Ti_{bedrock} are the corresponding titanium concentrations. Then, a negative τ value indicates that the element is lost during weathering, a τ value close to zero implies no loss or gain, whereas a positive τ value indicates a gain of the element. Note that τ values close to -1 means almost 100% chemical depletion during weathering.

The τ values of major, trace and rare earth elements for the weathered samples are shown in Table A.2 (in the Supplementary Material) and Fig. 8 (because of possible Na-rich fluid percolating, the τ values of Sample MB14–01 might have high uncertainties). The results show that Na and Ca have significantly negative τ values for the upper weathered samples and thus were mobile and leached during the early Eocene weathering. Elements Fe, Mg and Mn have positive τ values (Fig. 8), indicating enrichment of these elements in the upper layers, which is probably attributed to previous exposure and oxidation. Most of large ion lithophile elements (LILEs), such as Sr, Ba and Cs, have distinctly negative τ values for those weathered samples (Fig. 8), implying significantly chemical losses even under mild chemical weathering.

Although the weathered samples have roughly similar REE patterns with the fresh bedrock sample (Fig. 6), the light rare earth elements (LREEs), except Ce, have significantly more negative τ values (for instance, τ values of La are as low as -0.3 to -0.5) than middle and heavy rare earth elements (MREEs and HREEs) (Table A.2 and Fig. 8). This means that LREEs in granodioritic rocks are quite active and can be easily leached even under mild chemical weathering conditions, whereas MREEs and HREEs are relatively immobile. This finding implies that caution needs to be taken when using REE patterns (La_N/Yb_N) or LREE-related proxies (such as La/Th (Floyd and Leveridge, 1987) and Sm—Nd isotopes (McLennan et al., 1993)) to trace sedimentary provenance. For instance, the La_N/Yb_N and La/Th values display significant decreases with enhanced chemical weathering (Fig. 9). It is noteworthy that Ce has significantly higher τ values than La and Pr, indicating different geochemical behaviors from other LREEs (Fig. 8). The geochemical results demonstrate nearly no Ce anomaly (chondrite-normalized) in the fresh bedrock sample, while the upper weathered samples have obviously positive Ce anomalies (Table A.1 and Figs. 6, 9). The Ce/Ce* values of the analyzed samples show highly positive correlations with Mn and Fe contents (Fig. A2 in the Supplementary Material), which might suggest the preferential adsorption or coprecipitation of CeO_2 on Fe—Mn (hydro)oxides coatings in oxic environments compared to La and Pr (Braun et al., 1990; Mongelli, 1993; Su et al., 2017). Therefore, we favor the positive Ce anomalies are due to surface exposure and oxidation rather than silicate weathering. It is also consistent with previous studies on several modern granitoid weathering profiles which indicate that surface granitoid rocks have much higher Ce/Ce* values than the lower granitoid rocks, although the lower bedrocks experienced intensive chemical weathering (e.g. Bao and Zhao, 2008). By contrast, the τ values of Eu varies from -0.2 to 0, revealing very slightly chemical loss and have similar ranges with Sm and Gd. This implies that Eu is reasonably inactive during mild weathering of plagioclase. It is reinforced by the relationships between Eu/Eu* and CIA values, which indicate no changes of Eu/Eu* with increasing CIA values (Fig. 9).

5.3. Tectonic and paleoclimatic implications

As mentioned above, the early Eocene weathering profile underwent relatively intensive physical but mild chemical weathering alteration. Dominant smectite in neoformed weathering products (Fig. 4B) and low CIA and PIA values (Fig. 7) suggest that the weathering profile was in Zones III–IV of an idealized weathering profile, as shown in Fig. 10A. And the analyzed samples are plotted close to the regions of Zones III–IV in the A-CN-K diagram (Fig. 10B). We favor that the uncoupled chemical and physical weathering conditions were due to active tectonism during the early Eocene. This can be explained as follows. In tectonically active regions, mechanical erosion rates generally compare favorably with rates of chemical weathering and non-steady-state weathering occurs (Nesbitt et al., 1997). In this case, intensely weathered profiles cannot be developed, because the profile materials are eroded before chemical weathering can produce the mineralogy of highly weathered bedrock. Such conditions result in production of sediments with mineralogy and geochemistry reflecting incipiently weathered zones of profiles (Nesbitt et al., 1997). The published geochemical data of the early Eocene sedimentary rocks in the northern Qaidam basin (Jian et al., 2013b; Song et al., 2013), which indicate low CIA and PIA values, exactly suggest overwhelmingly mild chemical weathering intensities of their source regions (Fig. 10B). This means that the mild chemical weathering was a regional rather than a local condition in northern Tibet. It is well acceptable that the northern Tibet was located in active tectonic settings during the early Eocene and deformation initiated across the north margin of the plateau shortly

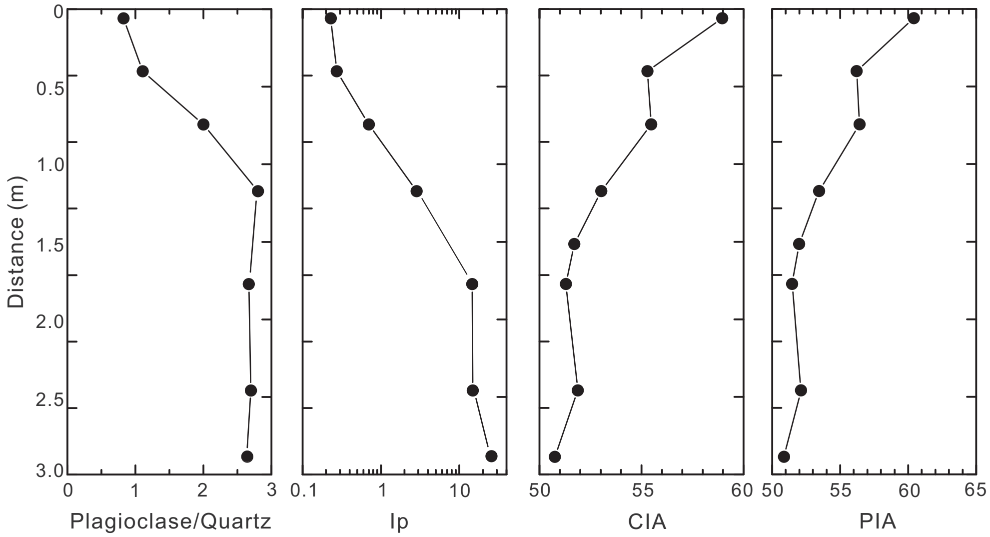

Fig. 7. Weathering indices of the analyzed paleoweathering profile. Note that plagioclase/quartz and Ip indices are based petrographic point-counting data and CIA and PIA values are calculated upon geochemical data.

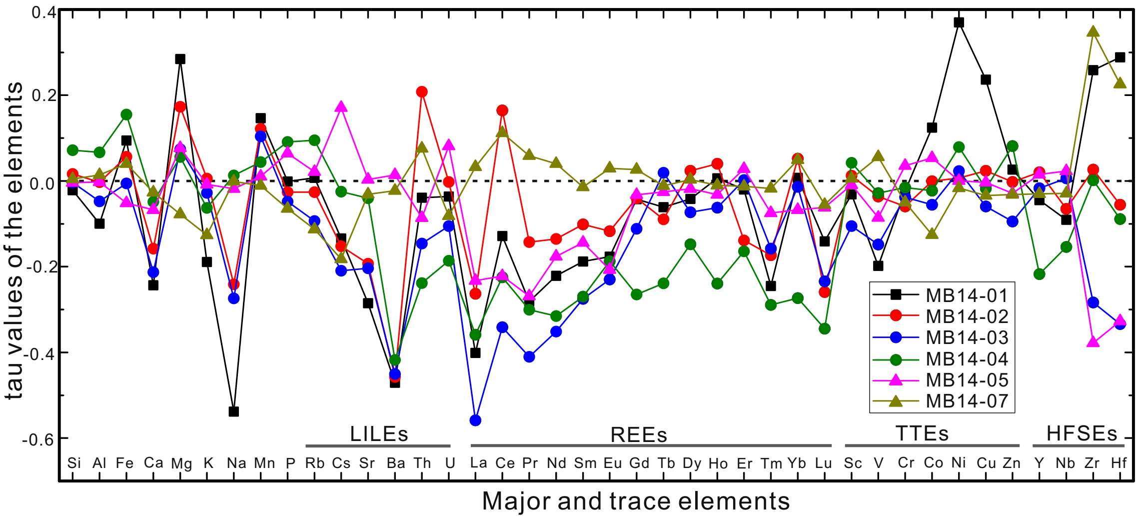

Fig. 8. Plots of τ values of the chemical elements. The τ values indicate concentration changes of elements in weathered samples in comparison to fresh bedrocks. The geochemical data of Sample MB14–06 are eliminated due to the apparent composition differences with the other two samples of the Layer 2, such as the significantly positive Eu anomaly, much lower abundances of some trace elements (e.g. Th, Sc, Nb and Cr) and relatively high plagioclase content for Sample MB14–06 (Table 1; Figs. 5–6). Note that the τ values of Sample MB14–01 might have high uncertainties because of possible Na-rich fluid percolation. LILEs: large ion lithophile elements; REEs: rare earth elements; TTEs: transition trace elements; HFSEs: high field strength elements.

after the India-Eurasia collision (e.g. Yin et al., 2008a; Clark et al., 2010; Duvall et al., 2011; Zhuang et al., 2011). And the early Eocene deformation in northern Tibet was a fast and short-lived event (Jian et al., 2018), which was probably a far-field response to the collision and thus made for intensive uplift and rapid erosion at that time.

Furthermore, the mild chemical weathering conditions could also be resulted from relatively dry climates (i.e. low supply of water) in northern Tibet during the early Eocene. The dominant smectite in the neoformed weathering products (Fig. 4B) also supports the dry climates, which tend to create poorly-drained conditions favorable for smectite formation during the weathering (e.g. Istok and Harward, 1982; Aoudjit et al., 1995; dos Santos et al., 2017). There was a Paleogene zonal arid band extending from East China to Central Asia due to a planetary-wind-dominant climate system (Liu and Guo, 1997; Sun and Wang, 2005; Zhang et al., 2007), and the northern Tibet was involved in. Previous pollen analysis results of the Qaidam basin demonstrated relatively high percentages of xerophytic taxa in the early Eocene sedimentary rocks (Wang et al., 1999), implying relatively dry climates prevailed during the weathering time of the analyzed profile. The dry climate condition is also supported by the widespread lacustrine carbonates (e.g. dolomite) and evaporite sediments (e.g. gypsum and halite) in the early Eocene strata of the basin (Wang et al., 2011; Guan and Jian, 2013; Guo et al., 2017).

The chemical loss of Al during weathering, as indicated by a decreasing trend of Al/Ti ratios with chemical weathering intensity (Fig. 9), might reveal low pH values for the early Eocene weathering solution (Nesbitt and Muir, 1988). This conclusion is also reinforced by the highly-leached LILEs (e.g. Sr, Ba and Cs) and the mobilized LREEs in the upper weathered layers (Figs. 8–9). Nesbitt (1979) has proposed that some REEs can be removed into solution from granodioritic rocks under acidic weathering conditions. Contributions of soil waters and organic acids produced by vegetation were possibly insignificant for the weathering solution, since soil and vegetation was undeveloped in the profile (Fig. 2). Rather, the acidic weathering conditions were most likely caused by extremely high atmospheric CO_2 level during the early Eocene (Sloan and Rea, 1995; Pearson and Palmer, 2000; Pagani et al.,

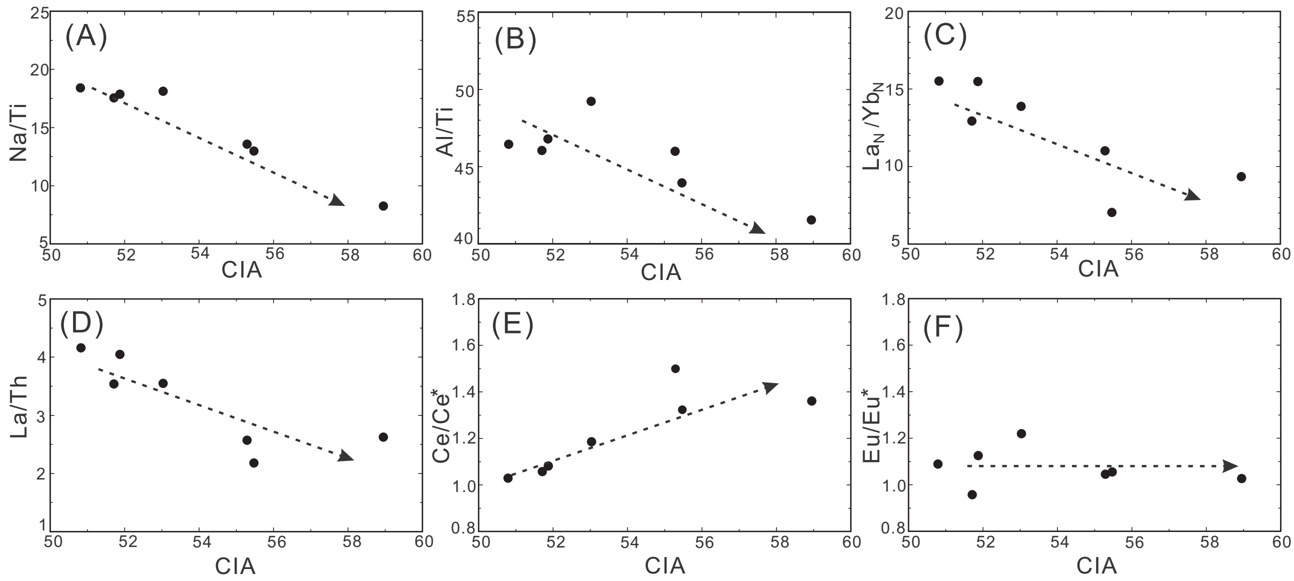

Fig. 9. Binary diagrams between elemental ratios and CIA values. Dashed arrows show the elemental ratio variations along with intensities of chemical weathering (i.e. CIA values).

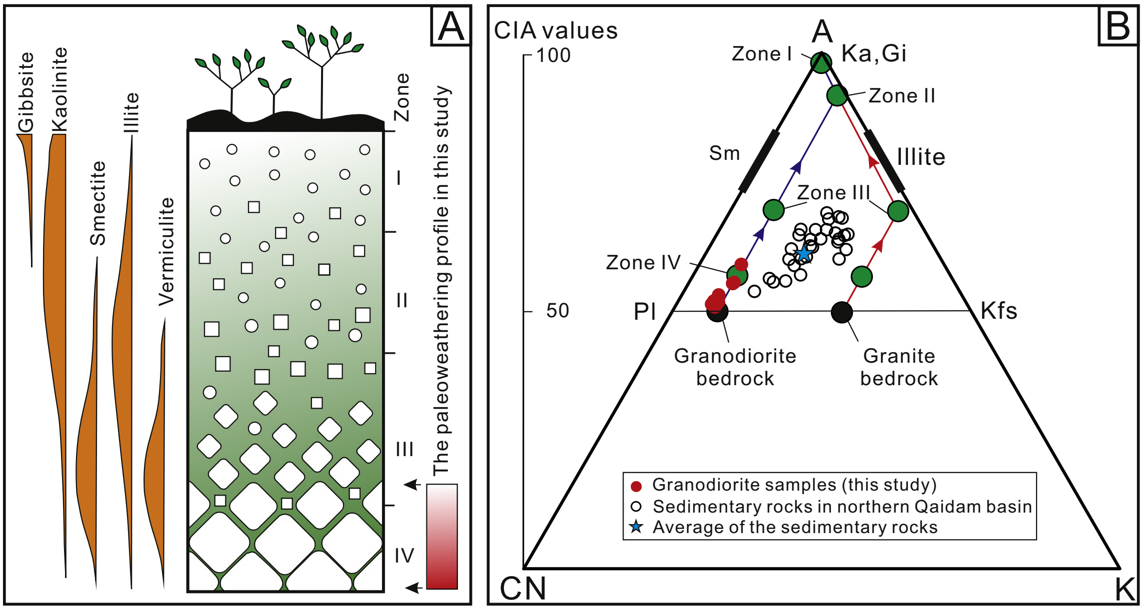

Fig. 10. (A) Clay mineral proportions and vertical zones of an idealized weathering profile developed on intermediate-acid igneous bedrock, modified from Nesbitt et al. (1997). (B) A-CN-K (Al_2O_3-(CaO + Na_2O)-K_2O in molecular proportions) ternary diagram for idealized weathering zones, analyzed granodiorite samples and early Eocene sedimentary rocks in northern Qaidam basin. Zone I, which is the most intensely weathered (steady-state weathering proposed by Nesbitt et al. (1997)), has abundant kaolinite and gibbsite in neoformed clay minerals and thus tends to plot close to the A apex in A-CN-K diagram. By contrast, Zone IV, immediately above fresh rock, is the least weathered and is characterized by a dearth of neoformed clay minerals (dominated by smectite or vermiculite if any) and thus plot close to the feldspar (Pl-Kfs) join line in A-CN-K diagram. Note that the paleoweathering profile in this study was most likely in Zones III–IV, and both sedimentary rock and paleoweathering profile data suggest mild chemical weathering conditions in northern Tibet during the early Eocene. Blue and red lines with arrows in the A-CN-K diagram represent predicted weathering trends of unweathered granodiorite and granite bedrock, respectively. Data of the early Eocene sedimentary rocks are from Jian et al. (2013b) and Song et al. (2013). Pl: plagioclase, Kfs: K-feldspar, Ka: kaolinite, Gi: Gibbsite, Sm: smectite. (For interpretation of the references to colour in this figure legend, the reader is referred to the web version of this article.)

2005; Lowenstein and Demicco, 2006). It is widely recognized that the atmospheric pCO_2 of early Eocene was probably as high as 1000 to 2000 ppmv (e.g. Pagani et al., 2005; Lowenstein and Demicco, 2006) and the greenhouse climate and pCO_2 were well coupled during that time (Zachos et al., 2008; Hyland and Sheldon, 2013). However, the mild chemical weathering degree of the analyzed profile (Fig. 7) suggests that the warm climate (i.e. high temperature) was probably not the major controlling factor for the early Eocene weathering in the northern Tibet.

6. Conclusions

The mineralogy, petrography and elemental geochemistry investigation of the granodioritic paleoweathering profile reveals the following conclusions:

1) Weathering indices based on geochemical data and dominant smectite in neoformed mineral phases indicate that the basement crystalline rocks underwent quite mild chemical weathering, whereas petrographic indices suggest that physical weathering played a significant role on the whole weathering process. This implies remarkable discrepancy between physical and chemical weathering alteration on the basement rocks. It is suggested that non-steady-state weathering, in which mechanical erosion rates compare favorably with rates of chemical weathering, prevailed in northern Tibet during the early Eocene.
2) This study provides a case to evaluate chemical element mobility of granodiorite weathering. The results indicate that most of LILEs, such as Sr, Ba and Cs, display significantly chemical loss during weathering. LREEs in granodioritic rocks are quite active and can be easily leached even under mild chemical weathering conditions, therein Ce shows positive anomalies due to surface oxidation. These findings imply that caution needs to be exercised when using LREE-related proxies to trace sedimentary provenance.
3) Large chemical losses of Al, LILEs and LREEs suggest an acidic weathering condition, which was probably a response to the extremely high atmospheric CO_2 level and greenhouse climates during the early Eocene. However, the regionally uncoupled chemical and physical weathering conditions were most likely attributed to dry climates governed by the Paleogene planetary-wind-dominant climate system and intensive tectonic deformation and erosion as a far-field response to the India-Eurasia collision.

Acknowledgments

This work is supported by National Natural Science Foundation of China (No. 41806052), Natural Science Foundation of Fujian Province (No. 2017J05067), Xiamen University Fundamental Research Funds for the Central Universities (No. 20720160114) and Internal program at the State Key Laboratory of Marine Environmental Science (No. MELRI1703). We would like to thank Drs. Yongshu Zhang, Daowei Zhang and Suotang Fu of PetroChina Qinghai Oilfield Company for their supports during the borehole sample collection. We also appreciate Dr. Fan Feng for their help in sample preparation and laboratory analysis. We are grateful to two reviewers for their thoughtful reviews that improved this manuscript.

Appendix A. Supplementary data

Supplementary data to this article can be found online at https://doi.org/10.1016/j.catena.2018.07.029.

References

An, Z., Kutzbach, J.E., Prell, W.L., Porter, S.C., 2001. Evolution of Asian monsoons and phased uplift of the Himalaya-Tibetan plateau since Late Miocene times. Nature 411, 62–66.

Aoudjit, H., Robert, M., Elsass, F., Curmi, P., 1995. Detailed study of smectite genesis in granitic saprolites by analytical electron microsopy. Clay Miner. 30, 135–147.

Banfield, J.F., Eggleton, R.A., 1990. Analytical transmission electron microscope studies of plagioclase, muscovite, and K-feldspar weathering. Clay Clay Miner. 38, 77–89.

Bao, Z., Zhao, Z., 2008. Geochemistry of mineralization with exchangeable REY in the weathering crusts of granitic rocks in South China. Ore Geol. Rev. 33, 519–535.

Berger, A., Janots, E., Gnos, E., Frei, R., Bernier, F., 2014. Rare earth element mineralogy and geochemistry in a laterite profile from Madagascar. Appl. Geochem. 41, 218–228.

Berner, R.A., 1995. Chemical weathering and its effect on atmospheric CO_2 and climate. Rev. Mineral. Geochem. 31, 565–583.

Bluth, G.J., Kump, L.R., 1994. Lithologic and climatologic controls of river chemistry. Geochim. Cosmochim. Acta 58, 2341–2359.

Braun, J.J., Pagel, M., Muller, J.P., Bilong, P., Michard, A., Guillet, B., 1990. Cerium anomalies in lateritic profiles. Geochim. Cosmochim. Acta 54, 781–795.

Braun, J.J., Pagel, M., Herbillon, A., Rosin, C., 1993. Mobilization and redistribution of REE and thorium in a syenitic lateritic profile – a mass-balance study. Geochim. Cosmochim. Acta 57, 4419–4434.

Cheng, F., Jolivet, M., Hallot, E., Zhang, D., Zhang, C., Guo, Z., 2017. Tectono-magmatic rejuvenation of the Qaidam craton, northern Tibet. Gondwana Res. 49, 248–263.

Clark, M.K., Farley, K.A., Zheng, D., Wang, Z., Duvall, A.R., 2010. Early Cenozoic faulting of the northern Tibetan Plateau margin from apatite (U-Th)/He ages. Earth Planet. Sci. Lett. 296, 78–88.

Condie, K.C., 1993. Chemical composition and evolution of the upper continental crust: contrasting results from surface samples and shales. Chem. Geol. 104, 1–37.

Condie, K.C., Dengate, J., Cullers, R.L., 1995. Behavior of rare earth elements in a paleoweathering profile on granodiorite in the Front Range, Colorado, USA. Geochim. Cosmochim. Acta 59, 279–294.

Di Renzo, F., Gabelica, Z., 1997. Barrerite and other zeolites from Kuiu and Kupreanof islands, Alaska. Can. Mineral. 35, 691–698.

Dixon, J.L., Hartshorn, A.S., Heimsath, A.M., DiBiase, R.A., Whipple, K.X., 2012. Chemical weathering response to tectonic forcing: a soils perspective from the San Gabriel Mountains, California. Earth Planet. Sci. Lett. 323, 40–49.

dos Santos, J.C.B., Le Pera, E., de Souza Júnior, V.S., Corrêa, M.M., de Azevedo, A.C., 2017. Gneiss saprolite weathering and soil genesis along an east-west regolith sequence (NE Brazil). Catena 150, 279–290.

Driese, S.G., Jirsa, M.A., Ren, M., Brantley, S.L., Sheldon, N.D., Parker, D., Schmitz, M., 2011. Neoarchean paleoweathering of tonalite and metabasalt: implications for reconstructions of 2.69 Ga early terrestrial ecosystems and paleoatmospheric chemistry. Precambrian Res. 189, 1–17.

Duvall, A.R., Clark, M.K., van der Pluijm, B.A., Li, C., 2011. Direct dating of Eocene reverse faulting in northeastern Tibet using Ar-dating of fault clays and low-temperature thermochronometry. Earth Planet. Sci. Lett. 304, 520–526.

Fedo, C.M., Nesbitt, H.W., Young, G.M., 1995. Unraveling the effects of potassium metasomatism in sedimentary rocks and paleosols, with implications for paleoweathering conditions and provenance. Geology 23, 921–924.

Floyd, P., Leveridge, B., 1987. Tectonic environment of the Devonian Gramscatho basin, south Cornwall: framework mode and geochemical evidence from turbiditic sandstones. J. Geol. Soc. Lond. 144, 531–540.

Foster, G.L., Vance, D., 2006. Negligible glacial-interglacial variation in continental chemical weathering rates. Nature 444, 918–921.

Fuentes, F., Aguirre, L., Vergara, M., Valdebenito, L., Fonseca, E., 2004. Miocene fossil hydrothermal system associated with a volcanic complex in the Andes of central Chile. J. Volcanol. Geotherm. Res. 138, 139–161.

Gaillardet, J., Dupré, B., Louvat, P., Allegre, C.J., 1999. Global silicate weathering and CO2 consumption rates deduced from the chemistry of large rivers. Chem. Geol. 159, 3–30.

Garzanti, E., Andò, S., France-Lanord, C., Vezzoli, G., Censi, P., Galy, V., Najman, Y., 2010. Mineralogical and chemical variability of fluvial sediments: 1. Bedload sand (Ganga–Brahmaputra, Bangladesh). Earth Planet. Sci. Lett. 299, 368–381.

Ghobarkar, H., Schaef, O., Guth, U., 1999. The morphology of hydrothermally synthesized stilbite type zeolites. J. Solid State Chem. 142, 451–454.

Gottardi, G., Galli, E., 2012. Natural Zeolites. Vol. 18. Springer Science & Business Media, pp. 1–411.

Guan, P., Jian, X., 2013. The Cenozoic sedimentary record in Qaidam basin and its implications for tectonic evolution of the northern Tibetan plateau. Acta Sedimentol. Sin. 31, 824–833 (In Chinese with English Abstract).

Guo, P., Liu, C., Yu, M., Ma, D., Wang, P., Wang, K., Mao, G., Zhang, Q., 2017. Paleosalinity evolution of the Paleogene perennial Qaidam lake on the Tibetan plateau: climatic vs. tectonic control. Int. J. Earth Sci. 1–16. https://doi.org/10.1007/s00531-017-1564-8.

Hodell, D.A., Mueller, P.A., Garrido, J.R., 1991. Variations in the strontium isotopic composition of seawater during the Neogene. Geology 19, 24–27.

Holland, H.D., Beukes, N.J., 1990. A paleoweathering profile from Griqualand West, South Africa: evidence for a dramatic rise in atmospheric oxygen between 2.2 and 1.9 bybp. Am. J. Sci. 290, 1–34.

Hyland, E.G., Sheldon, N.D., 2013. Coupled CO_2-climate response during the early eocene climatic optimum. Palaeogeogr. Palaeoclimatol. Palaeoecol. 369, 125–135.

Irfan, T.Y., Dearman, W.R., 1978. The engineering petrography of a weathered granite in Cornwall, England. Q. J. Eng. Geol. Hydrogeol. 11, 223–244.

Istok, J.D., Harward, M.E., 1982. Influence of soil moisture on smectite formation in soils derived from serpentinite. Soil Sci. Soc. Am. J. 46, 1106–1108.

Jacobson, A.D., Blum, J.D., Chamberlain, C.P., Craw, D., Koons, P.O., 2003. Climatic and tectonic controls on chemical weathering in the New Zealand southern Alps. Geochim. Cosmochim. Acta 67, 29–46.

Ji, J., Zhang, K., Clift, P.D., Zhuang, G., Song, B., Ke, X., Xu, Y., 2017. High-resolution magnetostratigraphic study of the Paleogene-Neogene strata in the northern Qaidam Basin: implications for the growth of the northeastern Tibetan plateau. Gondwana Res. 46, 141–155.

Jian, X., Guan, P., Zhang, D.-W., Zhang, W., Feng, F., Liu, R.-J., Lin, S.-D., 2013a. Provenance of Tertiary sandstone in the northern Qaidam basin, northeastern Tibetan plateau: integration of framework petrography, heavy mineral analysis and mineral chemistry. Sediment. Geol. 290, 109–125.

Jian, X., Guan, P., Zhang, W., Feng, F., 2013b. Geochemistry of Mesozoic and Cenozoic sediments in the northern Qaidam basin, northeastern Tibetan plateau: implications for provenance and weathering. Chem. Geol. 360, 74–88.

Jian, X., Guan, P., Zhang, W., Liang, H., Feng, F., Fu, L., 2018. Late Cretaceous to early Eocene deformation in the northern Tibetan plateau: detrital apatite fission track evidences from northern Qaidam basin. Gondwana Res. 60, 94–104.

Kump, L.R., Brantley, S.L., Arthur, M.A., 2000. Chemical weathering, atmospheric CO2, and climate. Annu. Rev. Earth Planet. Sci. 28, 611–667.

Lear, C.H., Elderfield, H., Wilson, P.A., 2003. A Cenozoic seawater Sr/Ca record from benthic foraminiferal calcite and its application in determining global weathering fluxes. Earth Planet. Sci. Lett. 208, 69–84.

Liu, T.S., Guo, Z.T., 1997. Geological environment in China and global change. In: An, Z. (Ed.), SelectedWorks of Liu Tungsheng. Science Press, Beijing, pp. 192–202.

Lowenstein, T.K., Demicco, R.V., 2006. Elevated Eocene atmospheric CO_2 and its subsequent decline. Science 313, 1928.

McDonough, W.F., Sun, S.S., 1995. The composition of the earth. Chem. Geol. 120, 223–253.

McLennan, S.M., 1989. Rare earth elements in sedimentary rocks: influence of provenance and sedimentary processes. Rev. Mineral. Geochem. 21, 169–200.

McLennan, S.M., Hemming, S., McDaniel, D.K., Hanson, G.N., 1993. Geochemical approaches to sedimentation, provenance and tectonics. Geol. Soc. Am. Spec. Pap. 284, 21–40.

Misra, S., Froelich, P.N., 2012. Lithium isotope history of Cenozoic seawater: changes in silicate weathering and reverse weathering. Science 335, 818–823.

Molnar, P., England, P., Martinod, J., 1993. Mantle dynamics, uplift of the Tibetan plateau, and the Indian monsoon. Rev. Geophys. 31, 357–396.

Mongelli, G., 1993. REE and other trace elements in a granitic weathering profile from "Serre", southern Italy. Chem. Geol. 103, 17–25.

Nedachi, Y., Nedachi, M., Bennett, G., Ohmoto, H., 2005. Geochemistry and mineralogy of the 2.45 Ga pronto paleosols, Ontario, Canada. Chem. Geol. 214, 21–44.

Nesbitt, H.W., 1979. Mobility and fractionation of rare earth elements during weathering of a granodiorite. Nature 279, 206–210.

Nesbitt, H.W., Muir, I.J., 1988. SIMS depth profiles of weathered plagioclase and processes affecting dissolved Al and Si in some acidic soil solutions. Nature 334, 336.

Nesbitt, H., Young, G.M., 1982. Early Proterozoic climates and plate motions inferred from major element chemistry of lutites. Nature 299, 715–717.

Nesbitt, H.W., Young, G.M., McLennan, S.M., Keays, R.R., 1996. Effects of chemical weathering and sorting on the petrogenesis of siliciclastic sediments, with implications for provenance studies. J. Geol. 104, 525–542.

Nesbitt, H.W., Fedo, C.M., Young, G.M., 1997. Quartz and feldspar stability, steady and non-steady-state weathering, and petrogenesis of siliciclastic sands and muds. J. Geol. 105, 173–191.

Pagani, M., Zachos, J.C., Freeman, K.H., Tipple, B., Bohaty, S., 2005. Marked decline in atmospheric carbon dioxide concentrations during the Paleogene. Science 309, 600–603.

Pearson, P.N., Palmer, M.R., 2000. Atmospheric carbon dioxide concentrations over the past 60 million years. Nature 406, 695–699.

Pe-Piper, G., 2000. Mode of occurrence, chemical variation and genesis of mordenite and associated zeolites from the Morden area, Nova Scotia, Canada. Can. Mineral. 38, 1215–1232.

Price, J.R., Velbel, M.A., 2003. Chemical weathering indices applied to weathering profiles developed on heterogeneous felsic metamorphic parent rocks. Chem. Geol. 202, 397–416.

Raymo, M.E., Ruddiman, W.F., 1992. Tectonic forcing of late Cenozoic climate. Nature 359, 117–122.

Riebe, C.S., Kirchner, J.W., Granger, D.E., Finkel, R.C., 2001. Strong tectonic and weak climatic control of long-term chemical weathering rates. Geology 29, 511–514.

Robert, C., Kennett, J.P., 1994. Antarctic subtropical humid episode at the Paleocene-Eocene boundary: clay-mineral evidence. Geology 22, 211–214.

Sloan, L.C., Rea, D.K., 1995. Atmospheric carbon dioxide and early Eocene climate: a general circulation modeling sensitivity study. Palaeogeogr. Palaeoclimatol. Palaeoecol. 119, 275–292.

Song, B., Zhang, K., Lu, J., Wang, C., Xu, Y., 2013. The middle Eocene to early Miocene integrated sedimentary record in the Qaidam Basin and its implications for paleoclimate and early Tibetan plateau uplift. Can. J. Earth Sci. 50, 183–196.

Su, N., Yang, S., Guo, Y., Yue, W., Wang, X., Yin, P., Huang, X., 2017. Revisit of rare earth element fractionation during chemical weathering and river sediment transport. Geochem. Geophys. Geosyst. 18, 935–955.

Sun, X., Wang, P., 2005. How old is the Asian monsoon system?—Palaeobotanical records from China. Palaeogeogr. Palaeoclimatol. Palaeoecol. 222, 181–222.

Wang, J., Wang, Y.J., Liu, Z.C., Li, J.Q., Xi, P., 1999. Cenozoic environmental evolution of the Qaidam Basin and its implications for the uplift of the Tibetan plateau and the drying of central Asia. Palaeogeogr. Palaeoclimatol. Palaeoecol. 152, 37–47.

Wang, C.W., Hong, H.L., Song, B.W., Yin, K., Li, Z.H., Zhang, K.X., Ji, J.L., 2011. The early-Eocene climate optimum (EECO) event in the Qaidam basin, northwest China: clay evidence. Clay Miner. 46, 649–661.

West, A.J., Galy, A., Bickle, M., 2005. Tectonic and climatic controls on silicate weathering. Earth Planet. Sci. Lett. 235, 211–228.

White, A.F., Blum, A.E., 1995. Effects of climate on chemical weathering in watersheds. Geochim. Cosmochim. Acta 59, 1729–1747.

Wilson, M.J., 2004. Weathering of the primary rock-forming minerals: processes, products and rates. Clay Miner. 39, 233–266.

Wu, H., Liu, C., Zhang, X., Ren, Z., 1997. Tectonic evolutions of Qaidam massif based on paleomagnetic measurements. Sci. China (Ser. D) 1, 9–14 (in Chinese).

Yin, A., Harrison, T.M., 2000. Geologic evolution of the Himalayan-Tibetan orogen. Annu. Rev. Earth Planet. Sci. 28, 211–280.

Yin, A., Dang, Y., Wang, L., Jiang, W., Zhou, S., Chen, X., Gehrels, G.E., McRivette, M.W., 2008a. Cenozoic tectonic evolution of Qaidam basin and its surrounding regions (part 1): the southern Qilian Shan-Nan Shan thrust belt and northern Qaidam basin. Geol. Soc. Am. Bull. 120, 813–846.

Yin, A., Dang, Y.Q., Zhang, M., Chen, X.H., McRivette, M.W., 2008b. Cenozoic tectonic evolution of the Qaidam basin and its surrounding regions (part 3): structural geology, sedimentation, and regional tectonic reconstruction. Geol. Soc. Am. Bull. 120, 847–876.

Yuan, D.-Y., Ge, W.-P., Chen, Z.-W., Li, C.-Y., Wang, Z.-C., Zhang, H.-P., Zhang, P.-Z., Zheng, D.-W., Zheng, W.-J., Craddock, W.H., Dayem, K.E., Duvall, A.R., Hough, B.G., Lease, R.O., Champagnac, J.-D., Burbank, D.W., Clark, M.K., Farley, K.A., Garzione, C.N., Kirby, E., Molnar, P., Roe, G.H., 2013. The growth of northeastern Tibet and its relevance to large-scale continental geodynamics: a review of recent studies. Tectonics 32, 1358–1370.

Zachos, J., Pagani, M., Sloan, L., Thomas, E., Billups, K., 2001. Trends, rhythms, and aberrations in global climate 65 Ma to present. Science 292, 686–693.

Zachos, J.C., Röhl, U., Schellenberg, S.A., Sluijs, A., Hodell, D.A., Kelly, D.C., Thomas, E., Nicolo, M., Raffi, I., Lourens, L.J., McCarren, H., Kroon, D., 2005. Rapid acidification of the ocean during the Paleocene-Eocene thermal maximum. Science 308, 1611–1615.

Zachos, J.C., Dickens, G.R., Zeebe, R.E., 2008. An early Cenozoic perspective on greenhouse warming and carbon-cycle dynamics. Nature 451, 279–283.

Zhang, Z., Wang, H., Guo, Z., Jiang, D., 2007. Impacts of tectonic changes on the reorganization of the Cenozoic paleoclimatic patterns in China. Earth Planet. Sci. Lett. 257, 622–634.

Zhuang, G., Hourigan, J.K., Ritts, B.D., Kent-Corson, M.L., 2011. Cenozoic multiple-phase tectonic evolution of the northern Tibetan plateau: constraints from sedimentary records from Qaidam basin, Hexi corridor, and Subei basin, northwest China. Am. J. Sci. 311, 116–152.